Energy & Environmental Science

Accepted Manuscript

This article can be cited before page numbers have been issued, to do this please use: L. Chen, X. Huang, Y. Cheng, Y. Fang, L. Zhang, X. Hu, S. Y. Jeong, H. Zhang, H. Y. Woo and F. Wu, *Energy Environ. Sci.*, 2022, DOI: 10.1039/D2EE02392J.

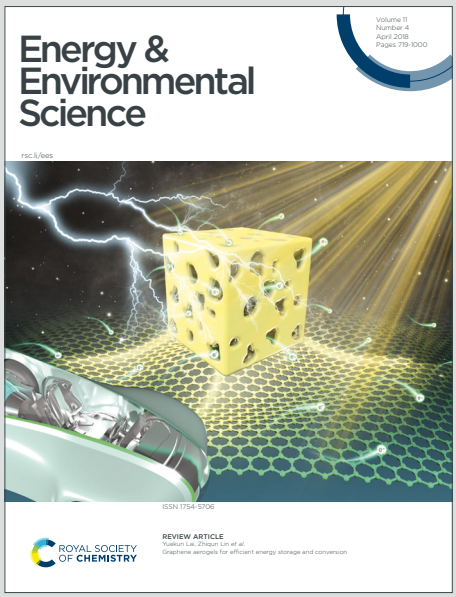




ROYAL SOCIETY OF CHEMISTRY

rsc.li/ees

View Article Online
DOI: 10.1039/D2EE02392J

The compromise between the power conversion efficiency (PCE) and the average visible transmittance (AVT) poses a big challenge when attempting to fabricate highly efficient semitransparent organic solar cells (ST-OSCs). Herein, we report a molecular weight-regulated efficient sequential deposition (SD) strategy, which is firstly employed to improve the performance of the ST-OSCs. Four batches of narrow bandgap polymer donor PCE10-2F with different molecular weights were synthesized. Simply regulating the molecular weights of the polymer is discovered to well balance independent film formation and miscibility of donor/acceptor interface during the SD process. Combined with the acceptor Y6 film optimized by dual additives, the overall performance of SD processed devices achieve superior performance compared to those of BC processed devices, thanks to the favorable morphology, optimized charge dynamics and reduced energy loss. Optical simulations reveal SD process favors a convenient and precise control of individual layer for optimization of light transmission with limited degradation in device performance. The corresponding ST-OSCs achieve high PCEs of 11.11%~10.01% and high AVTs of 39.93%~50.05%, showing breakthrough performance in ST-OSCs. More importantly, a successful balance of PCE and AVT produces a LUE of 5.01%, which is a champion value of ST-OSCs without complex optical engineering.

View Article Online
DOI: 10.1039/D2EE02392J

# Molecular Weight-regulated Sequential Deposition Strategy Enables Semitransparent Organic Solar Cells with Light Utilization Efficiency over 5%

Xuexiang Huang[a, 1], Yujun Cheng[a, 1] Yuan Fang[d], Lifu Zhang[b, 1], Xiaotian Hu[a], Sang Young Jeong[c], Hean Zhang[a], Han Young Woo[c], Feiyan Wu[a], Lie Chen[a,*]

[a] *Institute of Polymers and Energy Chemistry (IPEC)/College of Chemistry and Chemical Engineering, Nanchang University, Nanchang 330031, Jiangxi, China*

[b] *Institute of Advanced Scientific Research (iASR)/Key Lab of Fluorine and Silicon for Energy Materials and Chemistry of Ministry of Education, Jiangxi Normal University, Nanchang 330022, China*

[c] *S. Y. Jeong, Prof. H. Y. Woo Department of Chemistry College of Science Korea University 145 Anam-ro, Seongbuk-gu, Seoul 02841, Republic of Korea*

[d] *School of Future Technology, Nanchang University, Nanchang 330036, Jiangxi China*

[*]**Corresponding authors.**

*Email addresses:* chenlie@ncu.edu.cn (L. Chen)

[1] These authors contributed equally to this work.





## Abstract

The compromise between the power conversion efficiency (PCE) and the average visible transmittance (AVT) poses a big challenge for high performance

DOI: 10.1039/D2EE02392J

semitransparent organic solar cells (ST-OSCs). Herein, a molecular weight-regulated efficient sequential deposition (SD) strategy is firstly employed to improve the performance of the ST-OSCs. A series of narrow bandgap (NBG) polymer donors PCE10-2F with different molecular weights are synthesized. Molecular weight-regulated SD strategy is discovered to fine-tune the crystallinity of the polymers, not only favoring the formation of a dense and robust film, but also reasonably adjusting the compatibility of donor/acceptor to enhance interfacial contact. Thanks to the favorable morphology, efficient charge dynamics, and suppressed energy loss, a record PCE of 14.53% is obtained for the PCE10-2F/Y6 all-NBG materials-based opaque device. Optical simulations reveal that SD process favors a convenient and precise control of individual layers for optimization of light transmission. The corresponding ST-OSC achieves a breakthrough PCE of 11.11%~10.01% with a high AVT of 39.93%~50.05%. A champion light utilization efficiency (LUE) of 5.01% is achieved for ST-OSCs without complex optical engineering, demonstrating the successful balance of PCE and AVT. These results demonstrate that the molecular weight-regulated SD method is a facile and promising strategy for highly efficient ST-OSCs.

**Key words**: Semitransparent organic solar cells; Sequential deposition; Narrow bandgap; Light utilization efficiency

View Article Online
DOI: 10.1039/D2EE02392J





## 1. Introduction

Organic semiconductor materials have discontinuous absorption, which can selectively absorb invisible light wavelengths that the human eye cannot perceive, while transmitting visible light that the human eye can perceive. These features make organic semiconductors have unique advantageous in the preparation of semitransparent organic solar cells (ST-OSCs).[1-3] The application of ST-OSCs on architectural surfaces (e.g. panes, building facades) is very attractive and has been considered as a promising candidate for building integrated photovoltaics. [5-7] To date, the development of high-performance ST-OSCs is becoming the next research focus in the rapidly growing field of organic solar cells (OSCs). [8-12]

The power conversion efficiency (PCE) of ST-OSCs is far behind those of opaque devices, because apart from PCE, evaluation of ST-OSC device performance also needs to consider other key factors, including average visible transmittance (AVT), color rendering index (CRI), color coordinates, and color temperature.[13] Generally, for practical ST-OSC applications, the AVT value of ST-OSC devices should exceed at least 25% to meet the practical applications. [14-17] Actually, an AVT of 50% is the prerequisite for power-window application. [18] However, the ST-OSCs have such high AVT but still possess high efficiency are rarely reported. It is because the pursuit of high transmittance inevitably leads to low light utilization and photocurrent loss, causing a significant decrease in the PCEs. The compromise between the PCE and the AVT poses a big challenge when attempting to fabricate highly efficient ST-OSCs. Therefore, all-narrow bandgap (all-NBG) materials ($E_g^{opt}$ $\leqslant$1.6 eV) with strong absorption in the near-infrared (NIR) region are often selected as the active layer of ST-OSC, including NBG donors and NBG acceptors. [19] To more intuitively evaluate the comprehensive performance of ST-OSC, light utilization efficiency (LUE) (LUE = PCE × AVT) is used to assess the balance of PCE and AVT in a ST-OSC. [20-22] In recent years, ST-OSCs have made great progress by designing near-infrared absorption organic semiconductors, adjusting device structures, and developing high transparent electrodes. [23-27] For example, NBG acceptors with strong near-infrared absorption and good visible light transmission were developed for the multifunctional ST-OSC devices, such as colorful or infrared reflection of heat dissipation devices. [24, 28-29] To date, the advanced ST-OSC has achieved an

View Article Online
DOI: 10.1039/D2EE02392J

impressive PCE of 14.15%, but has a low AVT of 20.0% and a low LUE is only 2.83%.[30] Recently, favored by the combination of outcoupling coating with an anti-reflection layer, the LUE of the device has reached over 5.0%, but it required very complex optical engineering, which is conductive to mass production. [14,31]

In traditional ST-OSCs, one-step blend casting (BC) is the most prevalent method for the preparation of active layer, constructing bulk hetero-junction (BHJ) with molecularly mixed domains of the donor (D) and acceptor (A) materials. To achieve a highly efficient ST-OSC, besides maximizing the selective absorption of the invisible light, an ideal BHJ active layer must allow optimal charge dynamics, including fast exciton dissociation, efficient and balanced charge transport. However, the morphology of the BC active layers is very complex and highly relies on both intrinsic properties of the materials (e.g. solubility, aggregation, and D/A interfacial interaction) and the fabrication conditions (e.g. D:A ratio, solvents, and optimal treatment).[32] Therefore, precisely controlling the microstructures of the BC films to develop the favorably vertical distribution of the D:A blend (p-i-n structure) is a key challenge for BHJ solar cells. [33-36] In addition, the absorption of the donor is usually in or partly in the visible light region, thus regulation of the D/A ratio is appealing to improve AVT, however, the D/A in BHJ needs to be fixed in a certain ratio to obtain the best performance, severely limiting the independent optimization of each component in ST-OSCs. Moreover, the BHJ structure contains a large number of D/A interfaces that cause light scattering and parasitic absorption, resulting in the light loss in the devices. [37]

Sequential deposition (SD) technology is a two-step deposition to form quasi-layer-by-layer structure, where donor material and acceptor material are deposited sequentially. [38] Compared to BC, the SD has some unique advantages: (1) Donor and acceptor can be independently controlled and regulated, such as thickness, crystallinity, etc. (2) The SD processed active layer can enrich donor at the anode and acceptor at the cathode, thus forming an ideal vertical distribution of the D/A, which can improve the charge selectivity transport and suppress charge accumulation and recombination at interfaces. (3) The significantly reduced D/A interfaces can effectively reduce light scattering and parasitic absorption, improving the light transmission. [37, 39] However, there are still two key issues that should be addressed

for developing high performance SD devices. On one hand, both D and A materials should possess high crystallinity and self-standing film-forming property to prohibit the underlying layer from being washed away during the deposition process of the upper layer; On the other hand, moderate compatibility at the D/A interface is also critical to improve the D/A interaction and construct favorable p-i-n architecture for efficient charge dissociation and transport. [40] How to balance the above two contradictory issues are very crucial and still needs to be addressed for SD devices. Although the two-step SD method has been regarded as a potential alternative to the one-step BC method for producing highly efficient and stable OSCs, to date, research on the SD processed ST-OSCs is still limited.

Herein, we report a molecular weight-regulated efficient SD strategy, which is firstly employed to improve the performance of the ST-OSCs. Four batches of NBG polymer donor PCE10-2F with different molecular weights were synthesized. It is found that adjusting the molecular weight can fine-tune the crystallinity of the polymer donor, not only facilitating the formation of dense and robust films for efficient SD process, but also rationally control the compatibility of D/A to enhance favorable interfacial contact for charge dissociation and transport. Combined with the acceptor Y6 film optimized by dual additives, the selective absorption of the active layer in the invisible light region is further improved. The overall performance of SD processed devices achieve superior performance compared to those of BC processed devices, thanks to the favorable morphology, optimized charge dynamics and reduced energy loss. The SD processed PCE10-2F:Y6-based opaque device achieves a record PCE of 14.53%. At the same time, optical simulations reveal SD process favors a convenient and precise control of individual layer for optimization of light transmission with limited degradation in device performance. The corresponding ST-OSCs achieve high PCEs of 11.11%~10.01% and high AVTs of 39.93%~50.05%, showing breakthrough performance in ST-OSCs. More importantly, a successful balance of PCE and AVT produces a LUE of 5.01%, which is a champion value of ST-OSCs without complex optical engineering.

## 2. Results and Discussion

### 2.1 Optoelectronic Characterization

**Figure 1a** presents the chemical structures of PCE10-2F and Y6. A series of polymer donors (PCE10-2F) with different molecular weights were readily synthesized *via* Stille reaction by simply changing the reaction time. [13, 23] Experimental section of the Supporting Information gives the detailed synthesis and characterizations (**Figure S1**). The number-average molecular weights ($M_n$) of the four polymer donors are determined to be 32.4, 40.8, 53.3 and 61.1 kDa, and the polydispersity index (PDI) is 2.33, 2.04, 2.04 and 1.33, respectively (**Figure S2**, supporting information). According to the $M_n$, the four polymer donors are named as PCE10-2F-32.4kDa, PCE10-2F-40.8kDa, PCE10-2F-53.3kDa and PCE10-2F-61.1kDa.

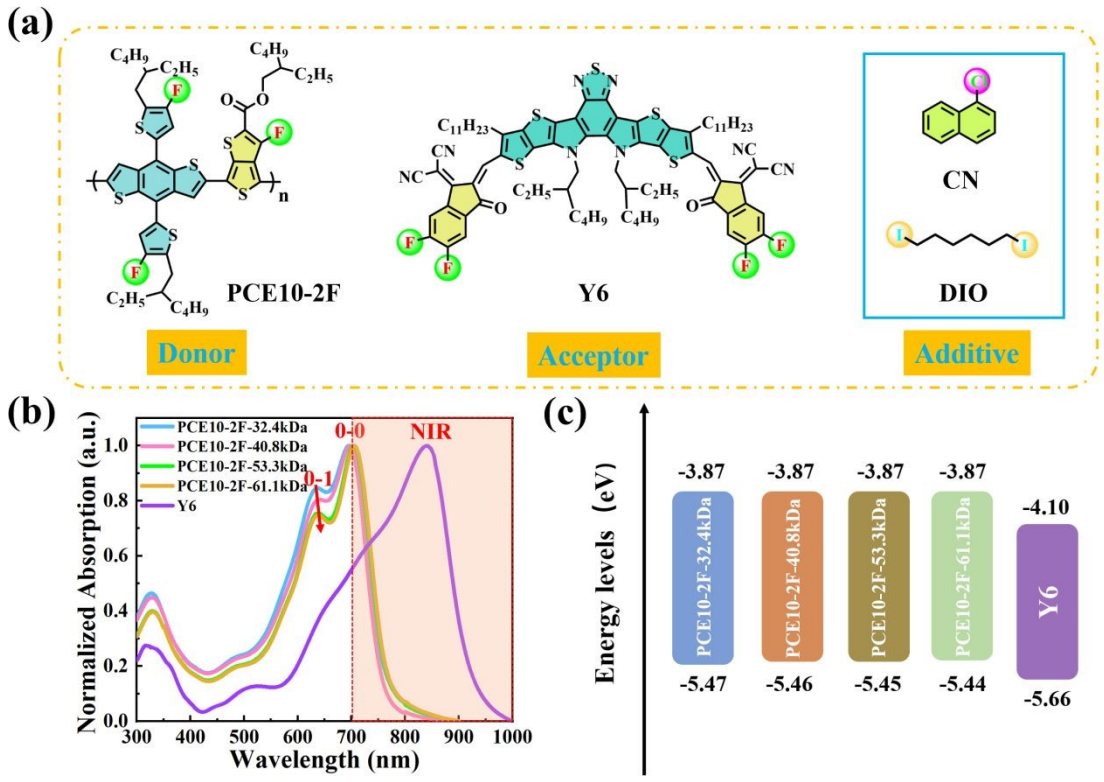


**Figure 1.** (a) Chemical structures of the polymer donor PCE10-2F, small molecular acceptor Y6, additives of CN and DIO. (b) Normalized UV-vis absorption spectra of PCE10-2F with different molecular weights and Y6 neat films. (c) Energy levels alignments of the polymer donors and Y6 acceptor.

UV-vis absorption spectra of pure PCE10-2F-32.4kDa, PCE10-2F-40.8kDa, PCE10-2F-53.3kDa, PCE10-2F-61.1kDa, and Y6 films are plotted in **Figure 1b**. It can be found that all the polymer donors have strong absorption in the range of 600-800 nm with maximum peaks at ~700 nm in the solid states, avoiding the sensitive band

region of the human eyes to solar light (400-700 nm). The donor and acceptor show complementary absorption, in favor of efficient light utilization. The optical and electrochemical parameters of polymer donors are listed in **Table S1**. The optical band gaps of PCE10-2F-32.4kDa, PCE10-2F-40.8kDa, PCE10-2F-53.3kDa, PCE10-2F-61.1kDa and Y6 calculated from the absorption spectra are 1.60, 1.59, 1.58, 1.57 and 1.33 eV, respectively. **Figure S3** shows the highest occupied molecular orbital (HOMO) and lowest unoccupied molecular orbital (LUMO) energy levels derived from cyclic voltammetry (CV). The $M_n$ has a slight impact on the energy levels of the polymers. In **Figure 1c, Figure S3** and **Table S1**, as $M_n$ increases from 32.4 to 61.1 kDa, the HOMO levels increase slightly.

### 2.2 Molecular Aggregation Properties

The molecular aggregation property of the active layer materials, especially of the underlying materials, is very important, even decisive for the SD processed devices. [41,39] To evaluate the molecular aggregation behaviors of the polymers, the temperature-dependent UV-vis absorption spectra of the PCE10-2F with different molecular weights were measured in chlorobenzene solutions (**Figure 2**, **Figure S4** and **Table S1**). The heating process of the polymer solutions was recorded from 20 °C to 100 °C (**Figure 2a-d**). The absorption curves of these four polymer donors have two absorption peaks: the 0-1 peak corresponds to intramolecular charge transfer, the 0-0 peak is related to molecular aggregation, and the ratio of $I_{0\text{-}0}/I_{0\text{-}1}$ reflects the relative strength of the molecular aggregation. [42] Four polymers display distinct 0-0 peaks with much higher intensity than the 0-1 peaks, especially at low temperature, which is attributed to the intense pre-aggregation of polymers in their solutions. As the temperature increases, the 0-0 peak gradually decreases, and both 0-1 and 0-0 peaks are blue-shifted, corresponding to the destruction of pre-aggregation of the polymers. **Figure 2i** shows the ratio of $I_{0\text{-}0}/I_{0\text{-}1}$ to estimate the aggregation degree. The $I_{0\text{-}0}/I_{0\text{-}1}$ values are 1.300, 1.398, 1.418 and 1.440 for PCE10-2F-32.4kDa, PCE10-2F-40.8kDa, PCE10-2F-53.3kDa and PCE10-2F-61.1kDa, respectively (**Table S1**). The gradually increase in $I_{0\text{-}0}/I_{0\text{-}1}$ reveals a progressively enhanced aggregation as the $M_n$ of the polymer increases. It is worth noting that the pre-aggregations in the polymer solutions with $M_n$ of 53.3 kDa and 61.1 kDa are less temperature-dependent and more

stable than the other counterparts, which can facilitate the formation of more dense thin films in actual devices. As revealed by **Figure 1c**, the molecular weights do affect the absorption profiles of these polymer donor films. With the increase of $M_n$, the 0-1 peaks of four polymers slightly red-shift, together with gradually increased the (0-0) peaks, as a result, the $I_{0-0}/I_{0-1}$ significantly increases (**Table S1**). These results indicate that increase of molecular weights induces stronger intermolecular interactions and higher crystallinity of the polymer films. We further compare the PCE10-2F with the state-of-the-art NBG polymer PCE10 and wide-bandgap polymer PM6 (**Figure S5**). Four PCE10-2F polymers all have more favorable aggregation behavior than PCE10 and PM6, beneficial for the fabrication of SD devices. **Figure 2e-h** show the absorption change of four polymers before and after being flushed with chloroform, a solvent used for deposition of the upper layer in SD process (see Supporting Information). Obviously, thanks to the high crystallinity and dense film induced by the high molecular weight, the absorption spectra of polymers with higher $M_n$ (PCE10-2F-53.3kDa and PCE10-2F-61.1kDa) hardly change before and after flushing, indicating good corrosion resistance of the polymers. On the contrary, the absorption intensity of polymers with lower $M_n$ (PCE10-2F-32.4kDa and PCE10-2F-40.8kDa) decreases significantly after chloroform flushing.

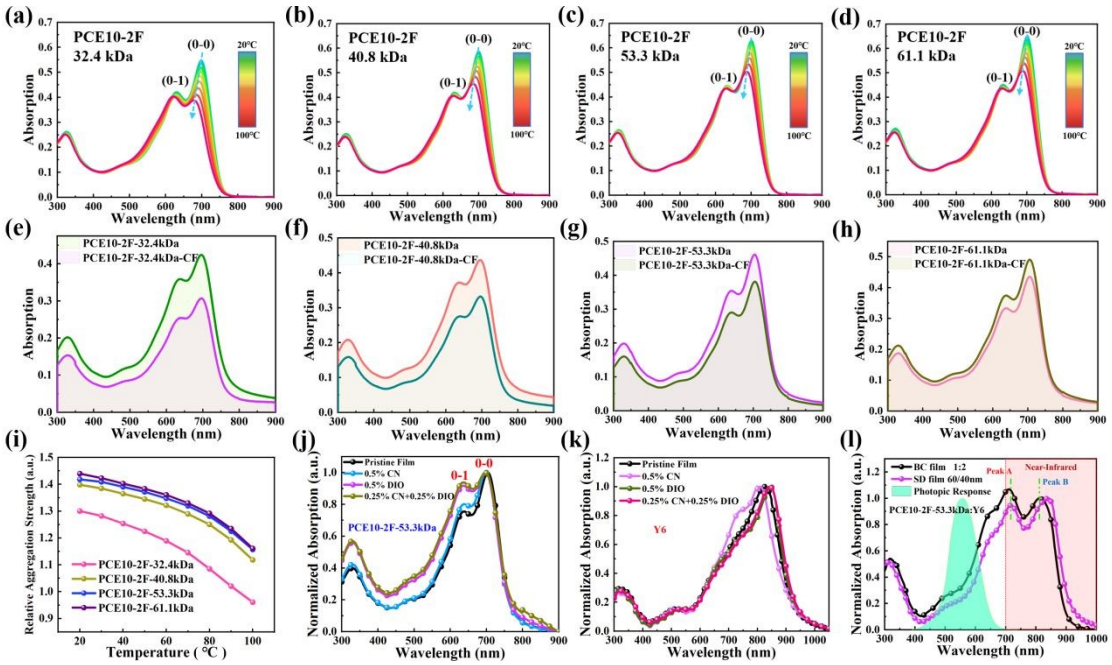


**Figure 2.** (a-d) Temperature-dependent UV-vis absorption spectra of 0.01 mg/mL polymer donor solutions. (e-h) the absorption spectra change of four polymers before

and after flushed with chloroform. (i) Plot of relative aggregation strength *versus* solution temperature. Normalized absorption spectra of (j) neat PCE10-2F-53.3kDa with and without CN or DIO additive, (k) neat Y6 with and without CN or DIO additive, and (l) optimal BC film (0.25% CN+0.25% DIO) and SD film (0.25% CN+0.25% DIO only for acceptor Y6).

Apart from regulation of the molecular weights, the use of additives is also an important treatment to tune the molecular aggregation. [43] It is well known that the crystallization and orientation of the photoactive materials are sensitive to solvent additives. The representative additives are 1-chloronaphthalen (CN) and 1,8-diiodooctane (DIO). Taking PCE10-2F-53.3kDa as an example, the normalized UV-Vis absorptions of PCE10-2F-53.3kDa after treated with different additives (0.5% CN, 0.5% DIO or 0.25% CN+0.25% DIO) are shown in **Figure 2j**. After normalization of the 0-0 peaks, all the 0-1 peaks of the additive-treated polymers increase with the decreased $I_{0\text{-}0}/I_{0\text{-}1}$ ratios, demonstrating that the additive treatment does not improve but reduce the crystallization of PCE10-2F. With DIO additive, prolonging the treating time causes significant destruction of molecular aggregation **(Figure S6)**. We further used the additives to regulate the molecular aggregation of acceptor Y6, as shown in **Figure 2k**. The pristine Y6 shows a maximum absorption peak at 825 nm. With the addition of CN, DIO or CN + DIO, the maximum absorption peak shifts to 809, 846 and 843 nm, respectively. Notably, compared with the blue-shift band of CN-treated Y6 film, the absorptions of DIO or CN+DIO-retreated Y6 films undergo a distinct red-shift (by 21 nm and 18 nm respectively), implying the improved crystallinity of the acceptor films. From **Figure 2j** and **Figure 2k**, it can be seen that the additive treatment does not improve but reduces the crystallization of PCE10-2F, while treatment of the acceptor with DIO or CN + DIO additives can achieve red-shifted absorption and improved crystallinity, so we speculated that additive-free donor and DIO or CN + DIO treated acceptor are more beneficial to achieve better device performance. **Figure 2l** compares the normalized UV-Vis absorptions of the BC film (CN+DIO) and SD film (CN+DIO only for acceptor Y6). The peak A of the BC and SD films assigned to the polymer donor PCE10-2F is at about 710 nm, while the peak B assigned to the acceptor Y6 exhibits a red shift by 30 nm for the SD film (840 nm) relative to the BC film (810 nm). These findings agree with the above UV observations of the individual polymer donor and

acceptor. Independently manipulating donor and acceptor by additives during the SD process achieves a superior absorption in the NIR region, which is beneficial to improve $J_{SC}$ but without affecting the AVT of ST-OSCs.

### 2.3 Molecular Orientation and Crystallinity

Molecular orientation and crystalline properties of neat polymer donor and acceptor were investigated by grazing incidence wide-angle X-ray scattering (GIWAXS) (**Figure 3**, **Table S2**). All pristine polymer films display a face-on oriented structure with significant scattering in the out-of-plane (OOP) (010) direction (**Figure 3a-d**). More importantly, the (010) scattering peaks of the polymers at a $q_z$ of 1.606-1.616 Å$^{-1}$, assigned to the π-π staking, become stronger and stronger as the $M_n$ increases from 32.4 kDa to 61.1 kDa. The corresponding *d*-spacing of PCE10-2F-32.4kDa, PCE10-2F-40.8kDa, PCE10-2F-53.3kDa and PCE10-2F-61.1kDa is 3.912 Å, 3.898 Å, 3.893 Å, and 3.888 Å, respectively (**Table S2**). Obviously, the gradually increased $M_n$ favors a closer π-π stacking, which will facilitate charge transport in the vertical direction. The crystallite coherence length (CCL) values are 9.845 Å, 12.017 Å, 12.516 Å and 13.620 Å for PCE10-2F-32.4kDa, PCE10-2F-40.8kDa, PCE10-2F-53.3kDa and PCE10-2F-61.1kDa, respectively. The crystal sizes also increase with the increase of $M_n$, which is consistent with the trend of polymer aggregation observed in temperature-dependent UV-Vis absorption spectroscopy. Therefore, the GIWAXS test illustrates that film aggregation and crystallinity have been well manipulated by controlling the molecular weights of the polymers.

The pristine Y6 film also exhibit a strong (010) peak and a weak (100) peak in the OOP and in-plane (IP) direction and direction, respectively, indicative of a preferential face-on orientation (**Figure 3e**).[44] After being treated with a mixture of 0.25% DIO and 0.25% CN additive, the diffraction (010) peak of Y6 film is shifted from 1.708 Å$^{-1}$ to 1.764 Å$^{-1}$, with the *d*-spacing decreasing from 3.679 Å to 3.562 Å (**Figure 3f** and **Table S2**). The related CCL of the double-additive-treated film is much longer than that of the pristine film (38.396 Å *vs* 24.44 Å). In particular, the double-additive-treated film emerges at a new peak at $q_z$=0.589 Å, suggesting the multi-scale ordered stacking of Y6 (**Figure 3g**). These signals of the GIWAXS measurement demonstrate the crystallinity of Y6 film after additive treatment has

been greatly improved, as confirmed by the red-shifted absorption band of the additive treated film in **Figure 2k**.

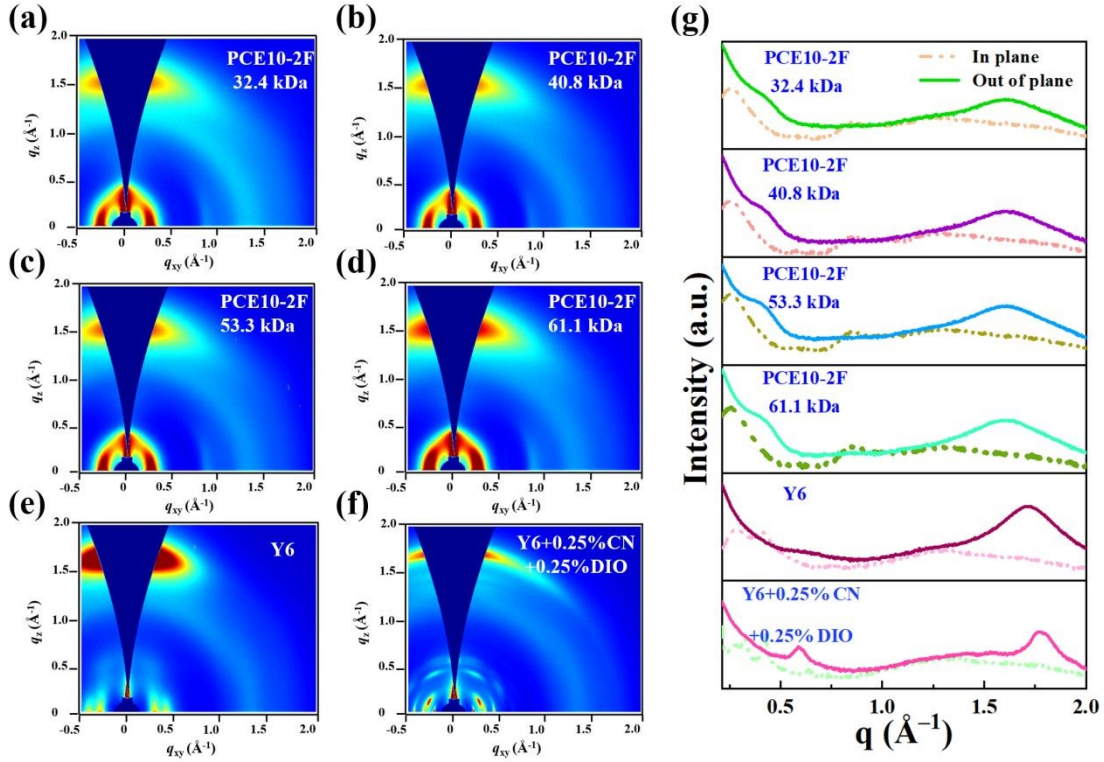


**Figure 3.** 2D GIWAXS profiles for neat (a) PCE10-2F-32.4kDa, (b) PCE10-2F-40.8kDa, (c) PCE10-2F-53.3kDa, (d) PCE10-2F-61.1kDa, (e) Y6 and (f) Y6 with 0.25%CN and 0.25%DIO based films. (g)1D GIWAXS intensity profiles along the in plane (dotted line) and out of plane (solid line) directions.

### 2.4 Traditionally Opaque Devices

To reveal the photovoltaic properties of the OSCs with PCE10-2F and Y6, the opaque devices were prepared by BC and SD process with a traditional device configuration of ITO/PEDOT:PSS/active layer/PDINO[45]/Ag. The structures of the active layer prepared by BC and SD methods are confirmed by cross-sectional scanning electron microscope (SEM) images, and schematic diagrams of BC, SD processing methods and the corresponding SEM images are shown in **Figure 4a-d**. The SD device exhibit a quasi-bilayer structure with a donor/acceptor interface (**Figure 4b**), whereas the BC device exhibit only a single active layer (**Figure 1d**). According to the results of UV observation in **Figure 2**, the strong corrosion resistance induced by high molecular weights can be effective against the washing from the upper layer, which is very

encouraging for a layer-by-layer deposition (**Figure 4e**). The active layer thickness of all BC and SD-OSCs is controlled at about 100 nm. Various optimization methods are performed to obtain the best device performance (**Figure S7** and **Table S3**). It is worth noting that the optimal donor/acceptor ratio of the processed by the BC method is 1:2, which is quite different from the 1:1.2 widely used in Y-series solar cells, which may be due to the unique photo-electronic property of PCE10-2F (**Figure 1c** and **Figure S4**). The accurate D/A ratio of the SD film is difficult to be evaluated. From the **Figure 2l** we can see that the profiles of the two films are similar, but the intensity of the polymer donor in SD film is slightly lower than BC film, indicating that the D/A is less than 1:2.

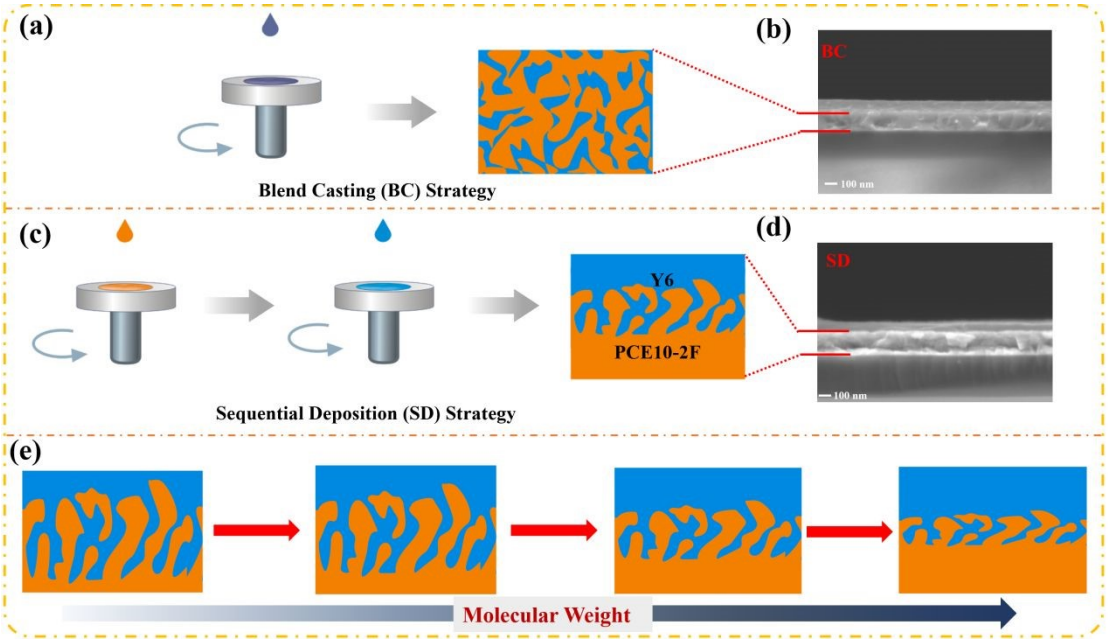


**Figure 4**. Schematic diagrams of (a, b) BC, (c, d) SD processing methods and the corresponding SEM images. (e) Demonstration diagram of molecular weight-regulated efficient SD strategy.

**Figure 5a** shows the schematic representation of final device structure. The *J-V* curves of performance optimal devices recorded under simulated AM1.5G sun illumination (100 mW $cm^{-2}$) are provided in **Figure 5b**, and the corresponding data is summarized in **Table 1**. According to the UV and GIWAXS results, for the SD devices, the polymer donor was deposited with no additive, but the acceptor Y6 was deposited with a mixture of 0.25%CN+0.25%DIO as an additive to obtain the best

performance. For the BC devices, the optimal fabrication condition is also with the 0.25%CN+0.25%DIO as additive. As shown in **Table 1**, the OSCs processed by the BC method performs similarly with PCEs ranging from 13.04% to 13.40%, indicating that the efficiency of BHJ devices is not sensitive to the batch of polymer PCE10-2F. However, the parameters of $V_{OC}$, $J_{SC}$ and FF of the BHJ devices show great difference. $V_{OC}$ decreases from 0.785V for PCE10-2F-33.4kDa to 0.773V for PCE10-2F-61.1kDa, resulting from their upshifted HOMO levels. The enhanced $J_{SC}$ with the $M_n$ increasing is relative to the increased extinction coefficient of the polymers (**Figure S4**). When using SD method to replace the BC method for devices fabrication, the PCEs of the devices are distinctly improved, due to the improved $V_{OC}$, $J_{SC}$ and FF. The SD processed devices show a saddle-like trend of the performance that rises first and then falls, as the $M_n$ of the polymers increases. Among these devices, the one based on PCE10-2F-53.3kDa performs best, delivering an outstanding PCE of 14.53%, which shows significant improvement over the device by BC process (PCE=13.40%). To the best of our knowledge, the PCE of 14.53% is the champion performance for all-NBG materials-based OSCs. Such high efficiency is also the best device performance based on PCE10-based polymers (**Table S4**). As shown in **Figure 5c**, compared with the BC processed OSCs, SD processed OSCs have significantly enhanced EQE responses in the NIR region (700-900nm), associated with their higher $J_{SC}$. The $J_{SC}$ values obtained from *J-V* curves (**Figure 5b**) are consistent with the external quantum efficiency (EQE) spectra (**Figure 5c** and **Figure S8**) integrated current densities, indicating the good reliability of the results.

View Article Online
DOI: 10.1039/D2EE02392J

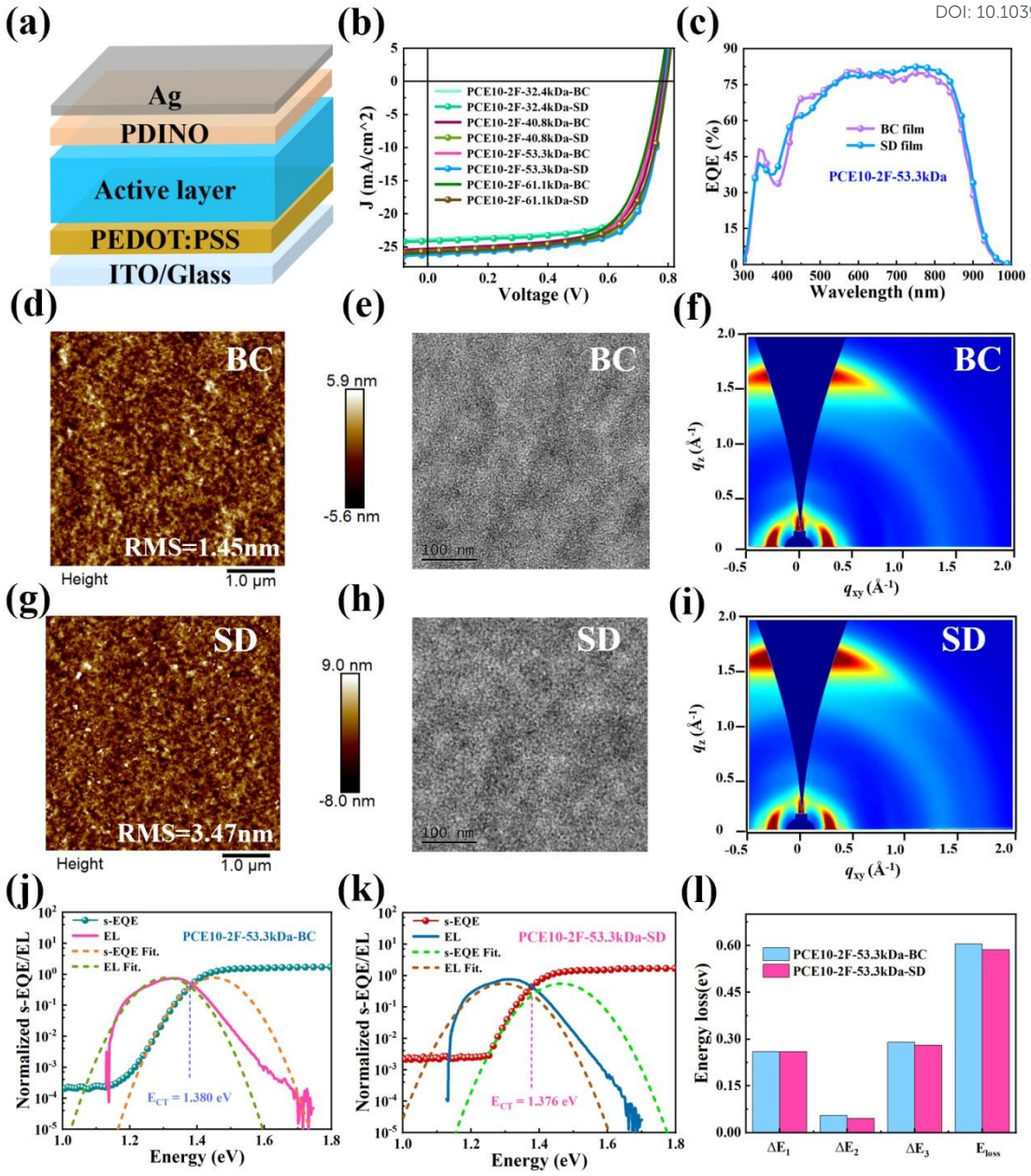


**Figure 5.** (a) Schematic representation of the final device structure. (b) *J-V* curves and (c) EQE spectra of the optimized opaque OSCs. (d, g) Tapping-mode AFM height images, (e, h) TEM images, (f, i) 2D GIWAXS patterns images and (h) in-plane and out-of-plane line cuts of GIWAXS of the optimized active layers (PCE10-2F-53.3kDa and Y6) based on BC and SD operating conditions. (j) Normalized sEQE and EL spectra of BC and (k) SD devices. (l) Comparison of energy loss in the BC and SD devices.

The charge dynamics were investigated to explain the $J_{SC}$ and FF difference between these devices. The space charge limited current (SCLC) method was performed to

detect the charge carrier transport in the devices (**Figure S9** and **Table S5**). As the molecular weight of PCE10-2F increases, both hole mobility ($\mu_h$) and electron mobility ($\mu_e$) of the device increase, which contributes to the improvement of $J_{SC}$. In addition, the SD devices show a better $\mu_h/\mu_e$ balance compared to the BC devices. More balanced charge mobilities demonstrate the reduced charge accumulation and recombination by SD process, accounting for the improved FF. Expectedly, among these polymers, PCE10-2F-53.3 kDa with highest $J_{SC}$ and FF shows the fastest and most balanced charge mobility. Charge recombination kinetics of the OSCs based BC and SD operating conditions were also probed by the $J_{SC}$ and $V_{OC}$ versus light intensity ($P_{light}$) (**Figure S10**). The decrease in the slopes of kT/q and α value approaching 1 confirm the suppressed biomolecular and trap recombination in SD device relative to BC device.

**Table 1.** Operating characteristics of opaque OSCs based on BC and SD processing method under simulated AM 1.5G, 100 mW $cm^{-2}$ illumination.

| Devices | Operating conditions | D/A | $V_{OC}$ (V) | $J_{SC}$ (mA/ $cm^2$) | FF (%) | PCE[(a)] (%) | AVT of active layer (%) |
|---|---|---|---|---|---|---|---|
| **PCE10-2F-33.4kDa** | BC | 1:2 | 0.785 | 23.82 | 69.86 | 13.11(12.90) | - |
| | SD | 60nm/40nm | 0.785 | 24.11 | 70.27 | 13.45(13.14) | - |
| **PCE10-2F-40.8kDa** | BC | 1:2 | 0.780 | 25.26 | 67.38 | 13.38(13.12) | - |
| | SD | 60nm/40nm | 0.791 | 25.58 | 70.48 | 14.27(13.91) | - |
| **PCE10-2F-53.3kDa** | BC | 1:2 | 0.775 | 25.82 | 67.07 | 13.40(13.09) | - |
| | **SD** | **60nm/40nm** | **0.789** | **26.14** | **70.32** | **14.53(14.15)** | **62.59** |
| | **SD** | **50nm/40nm** | **0.789** | **24.72** | **72.29** | **14.10(13.92)** | **66.23** |
| | **SD** | **40nm/40nm** | **0.790** | **23.61** | **72.39** | **13.51(13.21)** | **70.07** |
| **PCE10-2F-61.1kDa** | BC | 1:2 | 0.773 | 25.83 | 65.42 | 13.04(12.86) | - |
| | SD | 60nm/40nm | 0.794 | 25.70 | 67.70 | 13.82(13.40) | - |

(a)The values in parentheses stand for the average PCEs from 10 devices.

The increase of $V_{OC}$ is the main factor for the improvement in the PCEs of the SD processed devices than their corresponding BC processed ones. It has been reported that the DIO additive can promote the crystallinity and downshift LUMO of the acceptor Y6, leading to a distinct reduction in $V_{OC}$ of the devices.[46] We speculate that the $V_{OC}$ difference of OSCs between SD and BC process may be related to the effect of additives. Therefore, we investigated the effect of additive treatment on the performance of OSCs processed by SD and BC methods. The corresponding device

performance and parameters are shown in **Table S6**. For all the SD processed devices, when the donor is treated with the additive CN, there is little change in all performance parameters relative to the untreated devices, indicating that additive CN hardly affects the polymer donor. However, when the polymer donor is treated with the additive DIO, the PCEs of SD processed devices decrease significantly. These results are consistent with the UV observation. Intriguingly, in the case of SD processed PCE10-2F/Y6, the DIO additive exerts influence on both donor and acceptor, as revealed by the lower $V_{OC}$ of the DIO treated single layer (PCE10-2F or Y6) than the untreated devices, and the lowest $V_{OC}$ is obtained by the DIO treated double-layer (PCE10-2F and Y6). Similarly, the BC processed devices with DIO or CN+DIO additive all obtains relatively low $V_{OC}$ values. In addition, for SD processed OSCs, the $V_{OC}$ remarkably increases from 0.785V to 0.794V when molecular weights increase from 33.4 to 61.1kDa, which is probably due to that as the $M_n$ increases, the underlying donor forms a denser and more stable film to effectively avoid the penetration of DIO additive into the underlying donor layer. However, too dense and high crystallinity film will also reduce the interface area and the interaction between the underlying donor and upper acceptor, which strongly affects the charge generation and collection. Consequently, the PCE10-2F-61.1kDa with the highest molecular weight does not obtain the best performance but show inferior PCE of 13.82% together with reduced $J_{SC}$ and FF than PCE10-2F-53.3kDa, despite its highest $V_{OC}$ and robust film-forming property (**Figure 5b-d** and **Table 1**).

The top surface morphology of the blend films prepared by BC and SD methods was probed by atomic force microscopy (AFM) (**Figure 5d, Figure 5g** and **Figure S11**) and transmission electron microscopy (TEM) (**Figure 5e, Figure 5h** and **Figure S12**). As shown in **Figure S11**, when the $M_n$ of the donor PCE10-2F is 33.4kDa, smooth surfaces appear in both BC and SD processed active films, with root mean square (RMS) of 1.27 and 1.78 nm, respectively. The similar roughness indicates PCE10-2F-32.4kDa and Y6 have been mixed similarly in SD and BC processed film, due to the low corrosion resistance of PCE10-2F-32.4kDa. However, when the $M_n$ gradually increases to 61.1 kDa, the RMS of the BC processed films gradually increases to 2.28 nm and the phase separation becomes much larger, resulting from the gradually improved crystallinity of the polymer donor. The enlarged BHJ phase separation leads

to a lower FF along with the $M_n$ increase (**Figure S12**). The molecular weight-independence surface morphology is also observed for the SD films. In fact, for the SD processed films, the AFM probe the surface of the Y6. As the increase of the $M_n$, the surface morphology of the film deposited from the SD method becomes much rougher, and the highest RMS of 3.78 nm is obtained for PCE10-2F-61.1kDa/Y6 film, which is the closest to the surface of pristine Y6 film. This observation confirms that ideal vertical phase separation with p-i-n junction has been established in the BC processed blend films, which is conductive for efficient charge abstraction and suppressing charge recombination, consequently yielding the improved $J_{SC}$ and FF of SD-processed devices than their BC-processed counterparts (**Figure 5b** and **Table 1**). However, the PCE10-2F-61.1kDa with the highest crystallinity effectively defenses the erosion of the upper Y6 film and produces the most standard layer-by-layer structure, but the worst mutual compatibility between donor and acceptor is detrimental for optimization of the charge dynamics, accounting for its reduced PCE values (**Table 1**). **Figure 5f** and **5i** show the GIWAXS of the PCE10-2F-53.3kDa/Y6 and PCE10-2F-53.3kDa:Y6 films. In the BC film, a preferential face-on orientation is observed, with a prominent (100) peak at $q_{xy}$ = 0.0936 Å$^{-1}$ in the IP direction, and a (010) peak at $q_z$ = 1.700 Å$^{-1}$ in the OOP direction (**Figure S13**). However, in the SD film, there is a sharper (010) diffraction peak at $q_z$ = 1.710 Å$^{-1}$, associated with a *d*-spacing of 3.674 Å than that of BC film (3.696 Å). In addition, the SD film also has a larger CCL than the BC film (19.861 Å *vs* 18.452 Å). The tighter molecular packing and higher crystallinity of SD films is very helpful to enhance the charge transport. Moreover, the stacking of the films reflected by the morphology measurement is accordance with their light absorption of the films.

Furthermore, the detailed component energy loss ($E_{loss}$) was further quantitatively analyzed by sensitive external quantum efficiency (sEQE) and electroluminescence quantum efficiency ($EQE_{EL}$) experiments (**Figure 5j-l**, **Figure S13** and **Table 2**). According to the theory of detailed balance, $E_{loss}$ can be divided into three different components ($E_{loss}=\Delta E_1+\Delta E_2+\Delta E_3$). [47] The first part is the unavoidable energy loss ($\Delta E_1$), defined as the energy difference between the charge transfer state and the local excitation state of the donor or acceptor material. Devices based on BC and SD operating conditions have the same $\Delta E_1$ value (0.260 V). The second component ($\Delta E_2$)

is from the radiative recombination loss below the bandgap. SD device exhibits the lower non-ideal radiative attenuation value $\Delta E_2$ than BC device (0.046 V *vs* 0.055 V). The $EQE_{EL}$ of the SD device is $1.90\times10^{-5}$, while the BC device is $1.37\times10^{-5}$ (**Figure S14**) Thereby, the third part, non-radiative recombination loss ($\Delta E_3$) can be calculated to be 0.281V for SD device and 0.290V for BC device, according to the equation of $\Delta E_3 = -kTlnEQE_{EL}$ (k is Boltzmann constant, T is the room temperature). The much smaller non-radiative recombination loss of SD processed device may be related to the lower recombination energy from its more favorable morphology, accounting for its superior performance than BC processed device.

**Table 2.** Detailed energy loss of BC and SD processing method devices based on PCE10-2F-53.3kDa.

| Device | $E_g$ (eV) | $qV_{OC}$ (eV) | $qV_{SQ}$ $_{OC}$ (eV) | $qV_{rad}$ $_{OC}$ (eV) | $\Delta E_1$ (eV) | $\Delta E_2$ (eV) | $\Delta E_3$ (eV) | $E_{loss}$ (eV) | $EQE_{EL}$ (%) |
|---|---|---|---|---|---|---|---|---|---|
| BC | 1.380 | 0.775 | 1.123 | 1.068 | 0.260 | 0.055 | 0.290 | 0.605 | $1.37\times10^{-3}$ |
| SD | 1.376 | 0.789 | 1.123 | 1.077 | 0.260 | 0.046 | 0.281 | 0.587 | $1.90\times10^{-3}$ |

### 2.5 Absorption Selectivity Regulation and Simulation

Although the main absorption of the NBG active layer is located at NIR, the PCE10-2F still has some absorption in the visible region. To further optimize the transmittance of the active layer, we manipulate the thickness of the PCE10-2F-53.3kDa, in view of its best performance. **Figure 6a** presents the transmission spectra of active layers with different thickness of the donor, while keeping the same thickness of the acceptor. It can be found that reducing the thickness of the PCE10-2F is very helpful to improve AVTs of the active layer. Specifically, the thickness of PCE10-2F is reduced from 60 nm to 40 nm, the AVT of the active layer increases from 62.59% to 70.07%. In order to reveal how the thickness of donor affect the device performance of OSCs, we also prepared the corresponding opaque devices by SD method, and the performance parameters are shown in **Figure 6b** and **Table 1**. As the thickness of PCE10-2F is reduced, device parameters show different trends. The $V_{OC}$ remains almost unchanged, while the $J_{SC}$ gradually decreases, but the FF is improved. The reduced $J_{SC}$ is from the reduced amount of the photoactive materials,

and the increased FF is due to the reduced the internal resistance with decrease of thickness. The resulting PCE and AVT of the active layer are 14.53% and 62.59% for 60 nm PCE10-2F film, 14.10% and 66.23% for 50 nm PCE10-2F film, and 13.51% and 70.07% for 40 nm PCE10-2F film. The corresponding EQE spectra are shown in **Figure 6c**. It is obviously that as the thickness of the donor decreases, the EQE response of the devices is greatly reduced in the region of 400-700 nm, which corresponds to the weakened visible light absorption. Compared with the transmission spectra in **Figure 6a**, it can be clearly observed that the decrease in EQE response corresponds to the increase in transmittance, reflecting the trade-off between light utilization and light transmission in semitransparent device applications. Moreover, the response change in the near-infrared region (700-900 nm) is small, even if the thickness of PCE10-2F is reduced to 40 nm, it can still maintain a high EQE response of more than 70%. These results indicate that reducing the donor thickness can greatly improve the transmittance of the active films, but with less influence on the device efficiency (**Figure S15**), which is very beneficial for the preparation of highly efficient ST-OSCs.

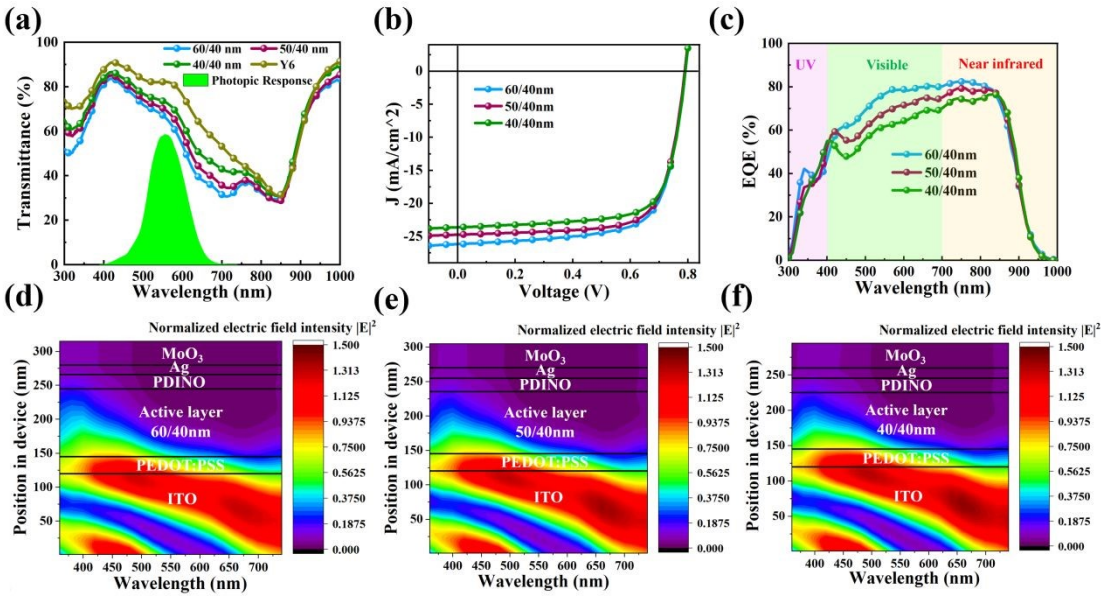


**Figure 6.** (a) Transmittance spectra of SD operating conditions films with different thickness (PCE10-2F-53.3kDa/Y6=60/40nm, 50/40nm, 40/40nm), (b) *J-V* curves, (c) EQE spectra of the SD processed opaque OSCs with different thickness. Simulated Electric field intensity $|E|^2$ of ST-OSCs by SD processing with D/A thickness of (d) 60/40nm (e) 50/40nm (f) 40/40nm.

Meanwhile, optical simulations were performed on the preparation of ST-OSCs under the above device conditions to analyze its optical loss. According to the curves of refractive index-n and extinction coefficients-k (acquired by the spectral ellipsometry technique) of active layer with wavelength according to different donor (40~60 nm) / acceptor (40nm) thickness ratio (**Figure S15**), the simulated electric field intensity $|E|^2$ under the ST-OSCs devices with the thickness of 60/40nm, 50/40nm, 40/40nm is shown in **Figure 6d-f**. Ag (15nm)/$MoO_3$ (35nm) electrode is chosen as transparent back electrode for optical simulation. All the SD processed ST-OSCs show weak light intensity distribution in visible light. This is because the reduction of D/A interface can effectively suppress light scattering and parasitic absorption, thereby reducing light loss in the device. [37] Obviously, the light intensity distribution varies with donor thickness. As the thickness of the donor decreased from 60 nm to 40 nm, the simulated electric field intensity in the visible region of 400-550 nm gradually decreases. These observations imply that the tuning the donor/acceptor thickness in the active layer by SD method is conductive to enhance the selective absorption of the device and improve the AVT of the devices.

### 2.6 Photovoltaic Performance of Semitransparent Devices

Inspired by the above results, PCE10-2F-53.3kDa is selected as the donor, and a series of SD processed ST-OSCs were fabricated by using normal structure of ITO/ PEDOT:PSS (25 nm)/active layer (80-100 nm)/PDINO (20 nm)/Ag (15nm)/$MoO_3$ (35 nm), with different donor thickness ratios (40~60 nm), as shown in **Figure 7a**. The *J-V* curves, transmittance spectra, transmittance spectra of the used electrode, reflectivity spectra and the corresponding EQE curves are shown in **Figure 7a-c** and **Figure S16**. The detailed device parameters are listed in **Table 3**. Compared with opaque devices, the ST-OSCs show decreased PCEs but increased AVT, due to the effect of the ultra-thin Ag electrode.[13] When the thickness of PCE10-2F-53.3kDa is 60 nm, the PCE of the ST-OSCs is 11.11%, $J_{SC}$ is 20.37 mA $cm^{-2}$, $V_{OC}$ is 0.785 V, FF is 69.48%, and AVT is 39.93%, giving a high LUE of 4.44%. As expected, the efficiency of ST-OSCs gradually decreases as the thickness of PCE10-2F-53.3kDa decreases, showing the same trends in opaque devices. At a thickness of 50 nm, PCE10-2F-53.3kDa/Y6 device provides a PCE of 10.56% and an AVT of 45.62%, yielding a notable LUE of 4.82%. Encouragingly, when the thickness of PCE10-2F-

53.3kDa is reduced to 40 nm, the device still obtains a competitive PCE of 10.01% and a prominent AVT of 50.05%. Consequently, the best LUE of 5.01% is achieved. **Figure 7d-e** and **Table S7-8** displays the comparison of our results with those reported in recent literatures. It clearly shows that all the PCEs of the ST-OSCs are the highest values with the AVT over 37%. More importantly, the LUE value of ST-OSCs is the champion value without complex optical engineering. These results demonstrate that a good balance of PCE and AVT has been achieved in these devices (**Figure 7f**). Additionally, the PCE10-2F-53.3kDa/Y6 (40/40) ST-OSC device shows a clear and bright background (**Figure S17**). This means that when ST-OSC is used as a power generation window, no additional artificial lighting is required, as its high AVT for efficient transmission of natural sunlight. We further studied the influence of molecular weight on ST-OSC devices (**Figure S16** and **Table S9**). We found that the variation trend of photovoltaic performance of ST-OSC devices with different molecular weights is very similar to those of opaque devices. Furthermore, quantum utilization efficiency (QUE) (QUE=EQE+T, T is the transmittance) was used to elucidate the light energy utilization of ST-OSCs. Note that the QUE values generally should be below 90% in the entire spectral region.[14] From **Figure S16** we can see that, the maximum EQE+T of these devices is 87%, confirming the reliability of these values.

View Article Online
DOI: 10.1039/D2EE02392J

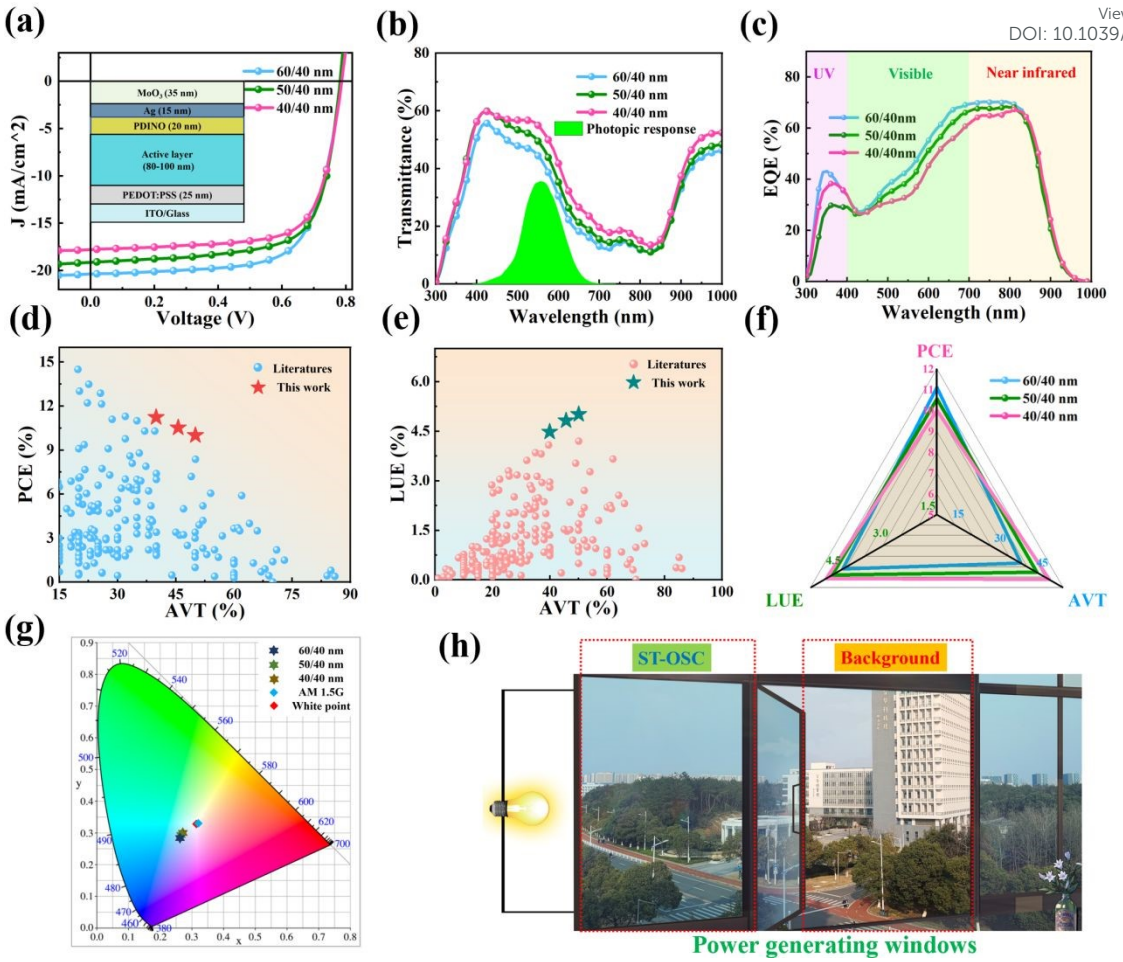


**Figure 7.** (a) Schematic of the semitransparent device and *J-V* curves, (b) Transmittance curves, (c) EQE curves of the ST-OSCs with different thickness active layers, error bars represent the standard deviation of the arithmetic mean of 10 devices. Comparison of our results with the (d) AVT and (e) LUE reported in the literatures without complex optical engineering. (f) Parameter comparison of 60/40 nm, 50/40 nm, 40/40 nm-based ST-OSCs. (g) Color coordinates of ST-OSC devices on a CIE 1931xy chromaticity diagram. (h) Power generating windows application scenario simulated by using background and ST-OSC filtered photos.

Besides the PCE and AVT, human color perception also should be considered and evaluated when ST-OSCs act as power generation windows.[13] Color perception can be expressed in color coordinates. The transmission spectra of ST-OSCs are used to calculate the color coordinates, and the corresponding results are plotted on the CIE 1931 (x, y) chromaticity diagram (**Figure 7g**). Moreover, the correlated color temperature (CCT) is also given for evaluating the optical properties of ST-OSCs. The CIE (x, y) color coordinates of devices (60/40 nm, 50/40 nm, 40/40 nm) are

located at (0.260, 0.279), (0.262, 0.285) and (0.265, 0.290), respectively, associated to the CCT of 13 368, 12 435, and 11 615 K, respectively (**Table 3**). Obviously, as the thickness of the donor PCE10-2F decreases, the color coordinates are closer to the white point (0.313, 0.329) and AM 1.5 G (0.320, 0.332), indicating that the color is closer to the neutral color, due to the smoother transmission of the active layer between 400-580nm. **Figure S17** shows a photo of the SD-processed devices (40/40 nm) put in front of the Nanchang University campus buildings and landscape. After stitching with the background photo, the power generation windows application scene is simulated, which is shown in **Figure 7h**. Compared with the background photo, the buildings and scenery can be clearly seen through ST-OSC with small visual differences, implying the good aesthetics and transparency of the device.

**Table 3.** Operating characteristics of ST-OSCs based on PCE10-2F-53.3kDa/Y6 under simulated AM 1.5G, 100 mW $cm^{-2}$ illumination.

| Thickness (D/A) | $V_{OC}$ (V) | $J_{SC}$ (mA/ $cm^2$) | $J_{SC}^{cal}$ (mA/ $cm^2$) | FF (%) | PCE[a] (%) | AVT[b] (%) | LUE[c] (%) | CIE 1931(x.y) |
|---|---|---|---|---|---|---|---|---|
| 60/40nm | 0.786 | 20.37 | 19.25 | 69.48 | 11.11(10.98) | 39.93(37.96) | 4.44(4.38) | 0.260, 0.279 |
| 50/40nm | 0.783 | 19.14 | 18.29 | 70.33 | 10.56(10.41) | 45.62(43.12) | 4.82(4.48) | 0.262, 0.285 |
| 40/40nm | 0.786 | 17.79 | 16.87 | 71.44 | 10.01(9.79) | 50.05(47.28) | 5.01(4.63) | 0.265, 0.290 |

(a, b, c) The values in parentheses stand for the average from 10 independent devices.

## 3. Conclusions

In this manuscript, we demonstrate a molecular weight-regulated efficient SD method for the formation of the active layer to achieve high-efficiency ST-OSCs. Simply regulating the molecular weights of polymer donor PCE10-2F is discovered to well balance independent film formation and miscibility of donor/acceptor interface during the SD process. In addition, the NBG small molecule acceptor Y6 is well-optimized using dual additives for higher crystallinity with larger CCL. Consequently, with independent optimization of donor and acceptor, the overall performances of the SD devices are much better than those of the BC counterparts, due to the favorable morphology, optimized charge dynamics, and reduced energy loss. PCE10-2F-

53.3kDa/Y6 obtains an impressive PCE of 14.53% for the opaque device, which is the highest PCE reported for all-NBG OSC devices. Furthermore, independent regulation of each layer by the SD process favors a convenient optimization of light transmission. As a result, the corresponding ST-OSCs achieve PCEs of 11.11%~10.01% with an AVT of 39.93%~50.05%, all of which are the record values of ST-OSCs. Note that, without complex optical engineering, a champion LUE of 5.01% is obtained, indicating the successful balance of PCE and AVT. These findings demonstrate that molecular weight-regulated SD method is a facile and promising strategy for highly efficient opaque and ST-OSCs.

## AUTHOR INFORMATION

Corresponding Author

* E-mail: chenlie@ncu.edu.cn (L. Chen)

Notes

The authors declare no competing financial interest.

**Acknowledgements**

L. C. thanks for the support from the National Natural Science Foundation of China (NSFC) (51973087 and 52173170) and the Thousand Talents Plan of Jiangxi Province (jxsq2019201004). F. W. thanks for the support from the National Natural Science Foundation of China (NSFC) (22169012).

View Article Online
DOI: 10.1039/D2EE02392J

## REFERENCES

[1] H. Cheng, Y. Zhao and Y. Yang, *Adv. Energy Mater.,* 2022, **12**, 2102908.

[2] Y. Li, C. He, L. Zuo, F. Zhao, L. Zhan, X. Li, R. Xia, H. Yip, C. Li, X. Liu and H. Chen, *Adv. Energy Mater.,* 2021, **11**, 2003408.

[3] Z. Hu, J. Wang, X. Ma, J. Gao, C. Xu, K. Yang, Z. Wan, J. Zhang and F. Zhang, *Nano Energy* 2020, **78**, 105376.

[4] S. Dai and X. Zhan, *Adv. Energy Mater*. 2018, **8**, 1800002.

[5] Y. Bai, C. Zhao, X. Chen, S. Zhang, S. Zhang, T. Hayat, A. Alsaedi, Z. Tan, J. Hou and Y. Li, *J. Mater. Chem. A,* 2019, **7**, 15887-15894.

[6] T. Jian, G. Zhang, R. Xia, J. Huang, X. Li, M. Wang, Yip and Y. Cao, *Mater. Today Energy,* 2021, **21**, 100807.

[7] Y. Xie, Y. Cai, L. Zhu, R. Xia, L. Ye, X. Feng, H. Yip, F. Liu, G. Lu, S. Tan and Yanming Sun, *Adv. Funct. Mater.,* 2020, **30**, 2002181.

[8] K. Wu, H. Li and V. I. Klimov, *Nat. Photonics,* 2018, **12**, 105-110.

[9] Q. Xue, R. Xia, C. J. Brabec and H.-L. Yip, *Energy Environ. Sci*., 2018, **11**, 1688.

[10] G. Li, R. Zhu, Y. Yang, *Nat. Photonics,* 2012, **6**, 153-161.

[11] C. J. Traverse, R. Pandey, M. C. Barr and R. R. Lunt, *Nat. Energy,* 2017, **2**, 849-860.

[12] V. V. Brus, J. Lee, B. R. Luginbuhl, S. Ko, G. Bazan and T. Nguyen, *Adv. Mater.,* 2019, **31**, 1900904.

[13] X. Huang, L. Zhang, Y. Cheng, J. Oh, C. Li, B. Huang, L. Zhao, J. Deng, Y. Zhang, Z. Liu, F. Wu, X. Hu, C. Yang, L. Chen and Y. Chen, *Adv. Funct. Mater*., 2021, 2108634.

[14] G. P. Kini, S. J. Jeon, and D. K. Moon, *Adv. Funct. Mater*., 2021, **31**, 2007931.

[15] K.-S. Chen, J.-F. Salinas, H.-L. Yip, L. Huo, J. Hou and A. K. Y. Jen, *Energy Environ. Sci*., 2012, **5**, 9551.

[16] G. Xu, L. Shen, C. Cui, S. Wen, R. Xue, W. Chen, H. Chen, J. Zhang, H. Li, Y. Li and Y. Li, *Adv. Funct. Mater*., 2017, **27**, 1605908.

[17] M. B. Upama, M. Wright, N. K. Elumalai, M. A. Mahmud, D. Wang, C. Xu and

View Article Online
DOI: 10.1039/D2EE02392J

A. Uddin, *ACS Photonics,* 2017, **4**, 2327.

[18] Y. Li, X. Guo, Z. Peng, B. Qu, H. Yan, H. Ade, M. Zhang and S. R. Forrest, *Proc. Natl. Acad. Sci. U. S. A*., 2020, **117**, 21147.

[19] Xie Y, Xia R, Li T, L. Ye, X. Zhan, H. Yip and Y. Sun, *Small Methods,* 2019, **3**, 1900424.

[20] C. Yang, D. Liu, M. B. Bates and R. Lunt, *Joule,* 2019, **3**, 1803.

[21] Y. Li, C. Ji, Y. Qu, X. Huang, S. Hou, C. Li, L. Liao, L. J. Guo and S. R. Forrest, *Adv. Mater*., 2019, **31**, 1903173.

[22] Y. Xie, Y. Cai, L. Zhu, R. Xia, L. Ye, X. Feng, H.-L. Yip, F. Liu, G. Lu, S. Tan and Y. Sun, *Adv. Funct. Mater*., 2020, **30**, 2002181.

[23] X. Huang, J. Oh, Y. Cheng, B. Huang, S. Ding, Q. He, F. Wu, C. Yang, L. Chen and Y. Chen, *J. Mater. Chem. A,* 2021, 9, 5711-5719.

[24] Y. Cui, C. Yang, H. Yao, J. Zhu, Y. Wang, G. Jia, F. Gao and J. Hou, *Adv. Mater*., 2017, **29**, 1703080.

[25] W. Liu, S. Sun, S. Xu, H. Zhang, Y. Zheng, Z. Wei and X. Zhu *Adv. Mater*., 2022, 2200337.

[26] W. Liu, S. Sun, L. Zhou, Y. Cui, W. Zhang, J. Hou, F. Liu, S. Xu and X. Zhu. *Angew. Chem. Int. Edit.,* 2021. e202116111.

[27] P. Yin, Z. Yin, Y. Ma and Q. Zheng. *Energy Environ. Sci*., 2020, **13**, 5177-5185.

[28] T. Li, S. Dai, Z. Ke, L. Yang, J. Wang, C. Yan, W. Ma and X. Zhan, *Adv. Mater*., 2018, **30**, 1705969.

[29] B. Jia, S. Dai, Z. Ke, C. Yan, W. Ma and X. Zhan, *Chem. Mater*., 2017, **30**, 239.

[30] X. Yuan, R. Sun, Y. Wu, T. Wang, Y. Wang, W. Wang, Y. Yu, J. Guo, Q. Wu and J. Min, *Adv. Funct. Mater*., 2022, 2200107.

[31] X. Liu, Z. Zhong, R. Zhu, J. Yu and G. Li, *Joule*, 2022. https://doi.org/10.1016/j.joule.2022.06.009

[32] M. Li, Q. Wang, J. Liu, Y. Geng and L, Ye, *Mater. Chem. Front*., 2021, 5, 4851-4873.

[33] N. D. Treat, M. L. Chabinyc and *Annul. Rev. Phys. Chem.,* 2014, **65**, 59-81.

[34] Y. Huang, E. J. Kramer, A. J. Heeger and G. C. Bazan, *Chem. Rev.,* 2014, **114**,

View Article Online
DOI: 10.1039/D2EE02392J

7006-7043.

[35] S. Shoaee, M. Stolterfoht and D. Neher, *Adv. Energy Mater.,* 2018, **8**, 1703355.

[36] C. J. Schaffer, C. M. Palumbiny, M. A. Niedermeier, C. Jendrzejewski, G. Santoro, S. V. Roth and P. Muller-Buschbaum, *Adv. Mater.,* 2013, **25**, 6760-6764.

[37] S. Liu, H. Li, X. Wu, D. Chen, L. Zhang, X. Meng, L. Tan, X. Hu and Y. Chen, *Adv. Mater.,* 2022, 2201604.

[38] Z. Xiao, Y. Yuan, B. Yang, J. VanDerslice, J. Chen, O. Dyck, G. Duscher and J. Huang, *Adv. Mater*., 2014, **26**, 3068.

[39] X. Wang, L. Zhang, L. Hu, Z. Xie, H. Mao, L. Tan, Y, Zhang and Y. Chen, *Adv. Funct. Mater*., 2021, **31**, 2102291.

[40] H. Wang, P. Cheng, S. Tan, C. Chen, B. Chang, C. Tsao, L. Chen, C. Hsieh, Y. Lin, H. Cheng, Y. Yang and K. Wei, *Adv. Energy Mater*., 2021, **11**, 2003576.

[41] Y. Cui, S. Zhang, N. Liang, J. Kong, C. Yang, H. Yao, L. Ma and J. Hou, *Adv. Mater.,* 2018, **30**, 1802499.

[42] D. Liu, J. Mun, G. Chen, N. J. Schuster, W. Wang, Y. Zheng, S. Nikzad, J.-C. Lai, Yi. Wu, D. Zhong, Y. Lin, Y. Lei, Y. Chen, S. Gam, J. Chung, Y. Yun, J. B.-H. Tok and Z. Bao, *J. A. C. S.,* 2021, **143**, 11679-11689.

[43] Q. He, W. Sheng, M. Zhang, G. Xu, P. Zhu, H. Zhang Z. Yao, F. Gao, F. Liu, X. Liao and Y. Chen, *Adv. Energy Mater*., 2020, **11**, 2003390.

[44] J. Yuan, Y. Zhang, L. Zhou, G. Zhang, H. Yip, T.-K. Lau, X. Lu, C. Zhu, H. Peng, P. A. Johnson, M. Leclerc, Y. Cao, J. Ulanski, Y. Li and Y. Zou, *Joule,* 2019, **3**, 1140-1151.

[45] Z. Zhang, B. Qi, Z. Jin, D. Chi, Z. Qi, Y. Li and J. Wang, *Energy Environ. Sci*., 2014, **7**, 1966-1973.

[46] Q. Li, L. Wang, S. Liu, L. Guo, S. Dong, G. Ma, Z. Cao, X. Zhan, X. Gu, T. Zhu, Y. Cai and F. Huang, *ACS Energy Lett*., 2020, **5**, 3637-3646.

[47] G. Xu, H. Rao, X. Liao, Y. Zhang, Y. Wang, Z. Xing, T. Hu, L. Tan, L. Chen and Y. Chen, *Chinese J. Chem*., 2020, **38**, 1553-1559.